2024

Ca2+ binding shifts dimeric dual oxidase's truncated EF-hand domain to monomer

Chin-Chuan Wei
Southern Illinois University Edwardsville, cwei@siue.edu

Amena Razzak
Southern Illinois University Edwardsville

Hadis Ghasmi
Southern Illinois University Edwardsville

Biophysical Chemistry 312 (2024) 107271

Contents lists available at ScienceDirect

Biophysical Chemistry

journal homepage: www.elsevier.com/locate/biophyschem

Ca^{2+} binding shifts dimeric dual oxidase's truncated EF-hand domain to monomer

Chin-Chuan Wei [a,b,*], Amena Abdul Razzak [a,1], Hadis Ghasemi [a,1], Rahil Khedri [a], Alexandria Fraase [a]

[a] Department of Chemistry, College of Arts and Sciences, Southern Illinois University Edwardsville, Edwardsville, IL 62026, USA
[b] Department of Pharmaceutical Sciences, College of Pharmacy, Southern Illinois University Edwardsville, Edwardsville, IL 62026, USA

ARTICLE INFO

Keywords:
EF-hand
Calcium binding
NADPH oxidase
Dual oxidase
Fluorescence
Isothermal titration calorimetry

ABSTRACT

Hydrogen peroxide, produced by Dual Oxidase (Duox), is essential for thyroid hormone synthesis. Duox activation involves Ca^{2+} binding to its EF-hand Domain (EFD), which contains two EF-hands (EFs). In this study, we characterized a truncated EFD using spectrometry, calorimetry, electrophoretic mobility, and gel filtration to obtain its Ca^{2+} binding thermodynamic and kinetics, as well as to assess the associated conformational changes. Our results revealed that its 2nd EF-hand (EF2) exhibits a strong exothermic Ca^{2+} binding ($K_a = 10^7\ M^{-1}$) while EF1 shows a weaker binding ($K_a = 10^5\ M^{-1}$), resulting in the burial of its negatively charged residues. The Ca^{2+} binding to EFD results in a stable structure with a melting temperature shifting from 67 to 99 °C and induces a structural transition from a dimeric to monomeric form. EF2 appears to play a role in dimer formation in its apo form, while the hydrophobic exposure of Ca^{2+}-bound-EF1 is crucial for dimer formation in its holo form. The result is consistent with structures obtained from Cryo-EM, indicating that a stable structure of EFD with hydrophobic patches upon Ca^{2+} binding is vital for its Duox's domain-domain interaction for electron transfer.

1. Introduction

Reactive oxygen species (ROS), such as superoxide and hydrogen peroxide, play important roles in host defense, signal transduction, and hormone synthesis. ROS are generated enzymatically by NADPH oxidase (Nox) proteins. Several homologous enzymes have been identified, including Nox1–5, and Dual Oxidase 1 and 2 (Duox1 or Duox2) [1]. In recent years, evidence indicates that non-phagocytic cells require ROS production for proper functioning. Both deficiency or overproduction of ROS has been shown to lead to disease development, including neurological [2], cardiovascular [3], and renal [4] diseases. Moreover, the activity of Nox proteins in certain cells has been associated with antiviral immunity [5].

Nox family proteins exhibit similarity in topology but are activated and regulated differently. All Nox enzymes contain a transmembrane cytochrome *b*-type heme domain (TMD) linked to an NADPH- and FAD-flavoprotein or dehydrogenase domain (DH). In Nox1–3, the formation of a core enzyme flavocytochrome complex including auxiliary proteins is crucial for their ROS activity. Nox4 is the only enzyme that is constitutively active. On the other hand, Nox5 and Duox can be activated solely by Ca^{2+} through their additional self-contained EF-hand domains (EFDs). Duox possesses an additional peroxidase-like homology domain (PD), the precise function of which remains unclear. Duox1–2 are expressed in thyroid gland, where they generate hydrogen peroxide [6]. Hydrogen peroxide is then utilized by thyroid peroxidase to catalyze oxidative iodination and coupling, which are essential steps in thyroid hormone synthesis [7]. Moreover, recent evidences suggest that Duox also plays roles in innate immunity and signaling [8–10], and it is a potential therapeutic target for the treatment of allergic disease [9].

The precise mechanism by which Ca^{2+}-dependent Nox proteins are activated remains incompletely understood. Nox5 superoxide-generating activity involves interactions among its Ca^{2+}-bound EFD, TMD, and DH, allowing electron transfer from NADPH to FAD, then to hemes, and lastly to molecular oxygen. Upon Ca^{2+} binding, Nox5's EFD undergoes a conformational change that exposes hydrophobic patches and buries polar charged residues [11]. The Ca^{2+}-induced EFD-DH domain interactions in Nox5 have been demonstrated through the study of interactions between EFD and a regulatory EF-hand binding

* Corresponding authors at: Department of Chemistry, Southern Illinois University Edwardsville, 6 Hairpin Dr, Edwardsville, IL 62026-1652, USA.
E-mail address: cwei@siue.edu (C.-C. Wei).
[1] These authors have made equal contributions to this manuscript.

https://doi.org/10.1016/j.bpc.2024.107271
Received 15 December 2023; Received in revised form 17 April 2024; Accepted 22 May 2024
Available online 24 May 2024

domain (REFBD) peptide [12,13], as well as truncated Nox5 DH constructs [13]. However, studies of Duox are limited because the functional expression of Duox in non-thyroid cells is impeded by the requirement of an auxiliary protein, Duox Maturation Factor A (DuoxA), which is essential for promoting Duox membrane localization [14]. Both Duox and Nox5 contain structural EF-hand motifs (EFs) for Ca^{2+} binding. However, unlike Nox5, the study of Ca^{2+} binding to Duox has not been explored. An EF structural motif is a unique helix-loop-helix structure where the loop comprises 12 conserved residues at positions 1(+X), 3(+Y), 5(+Z), 7(−Y), 9(−X), and 12(−Z), which chelate a Ca^{2+} ion in a pentagonal bipyramidal geometry. Among the seven coordinates for Ca^{2+} binding, two are provided by a bidentate carboxylate group from the 12th residue, either Glu (E) or Asp (D). This binding arrangement is crucial for Ca^{2+} binding, as we have previously demonstrated that a single substitution of Glu with Gln (Q) completely abolishes the EF's ability to bind to Ca^{2+} [15,16]. Typically, an EF-hand is paired with another EF-hand, and two of these pairs are arranged in tandem to form a stable domain. One such example is calmodulin (CaM), which contains two EFs (EF1 and EF2) in its N-terminal half domain and EF3 and EF4 in is C-terminal half domain. These two half-domains are arranged into two dumbbell-like lobes connected by a flexible linker. In its Ca^{2+}-free state, CaM adopts a closed structure where the two lobes are in proximity, burying most of their hydrophobic residues. Upon Ca^{2+} binding, CaM undergoes a conformational change that extends its dumbbell-like structure and exposes its hydrophobic regions, allowing it to interact with target enzymes for activation. The dynamic nature of the central linker is essential for CaM's plasticity, enabling it to cooperate effectively in binding to target enzymes. Previously, we found that Nox5's EFD has similar Ca^{2+} binding and conformational changes as CaM [11]. However, Duox only contains two putative EFs and no REFBD sequence, suggesting a different activation mechanism from Nox5. In this study, we prepared a truncated EFD (residues 808–902; termed as EFD_S) of Duox1 and utilized fluorescence, calorimetry, electrophoresis mobility, light scattering, and gel filtration to determine its thermodynamics, kinetics, and the associated conformational changes. To investigate the role of each EF-hand, we prepared Ca^{2+}-site "knocking out" mutants and conducted identical characterization. Our results revealed that the apo form of Duox's EFD forms a dimer structure, and Ca^{2+} binding shifts its structure towards a monomeric form. The unexpected dimerization provides insight into the Ca^{2+}-induced conformational changes of EFD and its dynamic properties, essential for understanding the activation mechanism for Duox.

2. Experimental

2.1. General

All chemicals were purchased from MilliporeSigma (St. Louis, MO) and ThermoFisher Scientific (Waltham, MA). For buffers used in Ca^{2+} binding study, they were treated with Chelex-100 (Bio-Rad Laboratories, Hercules, CA) to remove any trace of Ca^{2+}. The protein concentrations were determined using Beer's law $A_{278} = \varepsilon bc$, where ε is the extinction coefficient, b is the path length in cm, and c is the concentration. The ε value of Trx-fused EFD_S and its mutants was calculated to be 27,960 M^{-1} cm^{-1}, based on their known numbers of tryptophan, tyrosine, and cystine residues, as determined previously [17]. The purity of all characterized proteins was at least 90% based on SDS-PAGE. Characterizations were repeated using a minimum of three distinct protein batches, and the results were reproducible.

2.2. Recombinant protein expression and purification

The truncated Duox1's EFD (residues 808–902) gene was PCR amplified with flanking *Kpn*I and *Xho*I sites and then ligated into a pThioHisA vector digested with same restriction enzymes. Mutagenesis was used to generate Ca^{2+} site knock-out mutants by substituting Glu (E) to Gln (Q) at the 12th residue of each EF-loop, as previously described [11]. The desired plasmids were transformed into the BL21(DE3) bacterial cell line (New England Biolabs, Ipswich, MA), which was induced with 0.3–0.5 mM isopropyl β-D-1-thiogalactopyranoside (IPTG) at OD_{600} = 0.4–0.6 for protein expression. The culture was incubated at room temperature with continuous agitation at 220 rpm for 18 h. The resulting His-patch thioredoxin (hpTrx) fused proteins were purified using an Immobilized Metal Affinity Chromatography (IMAC) column (Pro-bond, Invitrogen), followed by a Phenyl Sepharose column, as described previously [15], except for the double Ca^{2+} binding site knock-out mutant, which was purified using Fast Protein Liquid Chromatography (FPLC)-IMAC. The purified proteins were stored at -80 °C until use. To prevent spontaneous cysteine re-oxidation, we treated the samples with the reducing agent dithiothreitol (DTT) [18]. The protein samples were first treated with 10–40 mM DTT to reduce the cysteine residue, followed by buffer-exchanged with a buffer containing 1–2 mM DTT to keep the cystine residue in its reduced form. To rule out the possibility of cysteine reoxidation during characterization that could lead to erroneous conclusions, AEDANS-labeled EFD samples, prepared as described previously [15], were utilized to verify our results.

2.3. Isothermal titration calorimetry (ITC) and difference scanning calorimetry (DSC)

The binding measurements by ITC were performed on a MicroCal instrument (Malvern Panalytical, UK), as previously described [19]. Briefly, the Ca^{2+} titration was conducted by injecting 2–10 μL of a 1–2 mM Ca^{2+} (or 5–10 mM Mg^{2+}) solution sequentially into a sample cell (1.4377 mL) containing 0.025–0.050 mM protein in 50 mM Tris, pH 7.5, 1 mM DTT at 25 °C. The raw data was corrected for the heat of titrant dilution determined by conducting an experiment under identical conditions except no protein in the sample cell. The resulting binding isotherms were analyzed using the "one-set-of-sites" or "sequential-binding-sites" model in companion software. Note that the 1st titration data point was excluded from fitting due to instrument drift or other issues.

The DSC experiment was conducted on a MicroCal VP-DSC (Malvern Panalytical, UK), as previously described [13]. Briefly, the thiol-reduced samples (concentration ranged from 1 to 2 mg/mL) in 50 mM HEPES, 0.2 M NaCl, pH 7.5, and 1 mM DTT were placed in the sample cell with the reference cell containing identical buffer. The DSC was run at a heating rate of 60 °C/h. Each protein sample was initially scanned for the first cycle from 20 °C to the temperature before the 1st melting point (i.e., 45 °C and 55 °C for apo and Ca^{2+}-bound EFD_S) and cooled down to 20 °C followed by the second cycle from 20 to 90 or 120 °C. The resulting thermograms were fitted with two non-two-state functions to obtain the melting temperatures and unfolding enthalpies.

2.4. Spectroscopic measurements

Fluorescence spectra were recorded on a FluoroMax-4 or FluoroMax-3P (Horiba, Inc.). The 8-anilino-1-naphthalenesulfonic acid (ANS) fluorescence was excited at 350 nm and recorded from 400 to 650 nm, as described previously [19]. The kinetics were measured using a stopped-flow accessory SFA-20 (Tgk Scientific, Bradford-on-Avon, UK) attached to the FluorMax-3P [15]. To determine Ca^{2+} dissociation rate constant (k_{off}), a solution containing 2–5 μM Duox's EFD_S protein and 100 μM Ca^{2+} was rapidly mixed with a solution containing EDTA ranging from 10 to 20 mM EDTA at 25 °C in the presence of 200 μM ANS. The Ca^{2+} dissociation was monitored by ANS fluorescence decay at 480 nm, which was fitted with an exponential decay to obtain the value of k_{off}.

2.5. Gel filtration or size-exclusion chromatography (SEC)

The size exclusion chromatography was performed as previously described [20]. Briefly, EFD_S samples in a buffer containing 50 mM Tris,

pH 7.5, 0.25 M NaCl, 10–40 mM DTT, and 2 mM Ca^{2+} (or 2 mM EDTA) was injected into a Shodex PROTEIN KW802.5 column (Showa Denko America, *Inc*, New York) attached to Shimadzu HPLC system, The column was run with a buffer containing 50 mM Tris, pH 7.5, 0.25 M NaCl, and 2 mM Ca^{2+} or EDTA. To dissociate EFD dimer, 20 μL of the protein incubated in 2–4 M urea was injected into the HPLC column. The flow rate was set at 1.0 mL/min, and the UV detector was set to 280 nm. Before injection, the protein sample was filtered through a 0.45 μm filter and loaded into a 20-μL sample loop.

2.6. Dynamic light scattering (DLS)

The DLS experiments were performed on a DynaPro NanoStar (Wyatt Technology, Santa Barbara, CA), as described previously [20]. Briefly, the sample was filtered with a 0.1 μm filter before 20 μL of the sample at a concentration of 1–2 mg/mL in 50 mM Tris, pH 7.5, 1 mM DTT, and 2 mM Ca^{2+} or 1 mM EDTA was applied to a Wyatt disposable cuvette and left to equilibrate at 25 °C for 2 min. The acquisition time was set to 5 s and the minimum peak intensity was 1%. The hydrodynamic radius (R_h) and the molecular weight were calculated assuming the shape of molecules is spherical.

2.7. Computational

Homology modeling and computational calculations, such as electrostatic potential maps and accessible surface areas, were conducted as previously outlined [11,19]. The structures with Ca^{2+} and without Ca^{2+} were derived from the protein database (PDB) files: 7D3F.pdb and 7D3E.pdb for high and low concentrations of Ca^{2+}, respectively, except that Ca^{2+} ions and the missing sequences were added using homology modeling.

3. Results

3.1. Protein expression and purification

Based on topology analysis, the putative EF-hand domain (EFD) of Duox1 was identified from residues 751 to 1040. To express this domain, the gene was cloned and inserted into a pThioHisA vector, but the resulting EFD was expressed as inclusion bodies. Similarly, the EFD fused with bacterial thioredoxin (Trx) was also insoluble. Efforts to refold the protein only yielded a small amount of refolded protein, which was not sufficient for the intended biophysical characterization. Consequently, a shorter EFD construct consisting of two EF-hands motifs (residues 808–902; termed EFD_S) was prepared (Fig. 1). This truncated EFD was only expressed when fused with Trx. The removal of Trx by enterokinase rendered the protein unstable. Through the text, we refer to this Trx-fused truncated EFD (Trx- EFD_S) as EFD_S, unless it is necessary to specify the presence of the fused Trx protein.

To eliminate Ca^{2+} binding in the 1st EF, we substituted E839 with Q, resulting in the mutant named EFD_S(-EF1) to highlight its inability to binding Ca^{2+} in EF1, while EF2 retains the ability to bind Ca^{2+}. Similarly, we generated EFD_S(-EF2) and EFD_S(-EF1-EF2) mutants. EFD_S contains a single Cys residue and formed a dimer slowly through an intermolecular disulfide bond. However, the formation of this type of dimerization was prevented in the presence of reducing agents, such as DTT, or by covalently linking the Cys residue with a thiol-reactive fluorescent reagent, IAEDANS.

3.2. Ca^{2+} binding thermodynamics and kinetics

Since the intrinsic Trp and Tyr fluorescence cannot be used to determine Ca^{2+} binding, as the fluorescence did not change upon the addition of Ca^{2+} to Duox's EFD_S (data not shown), we used isothermal titration calorimetry (ITC) to determine the Ca^{2+} binding based on the heat evolved during the binding process. We observed a multi-phasic Ca^{2+} binding event for EFD_S, characterized by a strong exothermic binding, as indicated by the sharp transition and inflection point at approximately 1 molar ratio (Fig. 2A), followed by weak endothermal bindings. However, the binding isotherm cannot be fitted with a one-set-of-sites for two similar binding affinities or two-sequential-binding-sites model. Though the binding could be satisfactorily fitted with a five-sequential-binding model, the result of the fitting did not provide informative binding information. Despite this difficulty, the 1st Ca^{2+} binding can be satisfactorily fit with a one-set-of-sites model, yielding an association binding constant (K_a) of $2.51 \times 10^7\ M^{-1}$, a stoichiometry (n) of 0.92, and a heat of enthalpy (ΔH^o) of −10.80 kcal/mol (Fig. 3A).

To estimate the weak bindings, we added approximately 1 equivalent of Ca^{2+} to EFD_S to briefly saturate the first Ca^{2+} binding site before performing ITC titration. The resulting binding isotherm was represented for weak bindings, which can be fitted with a three-sequential-binding model with relatively weak binding affinities and enthalpy changes (Inserts, Fig. 1A). The K_a and ΔH^o values for such sequential bindings are $2.65 \times 10^{-5}\ M^{-1}$ and 1.22 kcal/mol; 1.71×10^{-4} and 3.29 kcal/mol; and $1.24 \times 10^{-5}\ M^{-1}$ and -3.09 kcal/mol, respectively. This suggests that EFD_S may contain non-specific Ca^{2+} binding sites and/or that our sample contained trace impurities. Nevertheless, the second Ca^{2+} binding appears to be weaker and evolves less heat.

The substitution of the 12th Glu residue with Gln in each EF loop completely abolished its Ca^{2+} binding, as previously published for Nox5 [11,16] and Duox [21]. Ca^{2+} titration to EFD_S(-EF1) resulted in a single binding event with a sharp transition occurring near a molar ratio of 1, reflecting a strong binding. The fitting yielded a K_a value of $1.25 \times 10^7\ M^{-1}$ with a ΔH^o value of −10.83 kcal ($n = 0.94$), using "one-set-of-sites" model (Fig. 2B). On the other hand, Ca^{2+} binding to EFD_S(-EF2) is weaker ($K_a = 5.46 \times 10^5\ M^{-1}$) and exhibited exothermically with ΔH^o of −1.22 kcal/mol (Fig. 2C). Therefore, we concluded that EF2 has a higher Ca^{2+} binding and the reaction is exothermic giving that the binding affinity and enthalpy change are similar in wild type and EFD_S(-EF1). On the other hand, EF1 displays weaker binding and small negative enthalpy change. Furthermore, we did not observe any additional weak Ca^{2+}-binding as in the wild type, indicating that the purified wild-type protein contains impure Ca^{2+}-binding protein(s) despite having been through IMAC and HIC columns. As expected, there were no Ca^{2+} binding to EFD_S(-EF1-EF2). Despite this finding, it is unclear whether there is cooperativity between two EFs for Ca^{2+} binding. Future

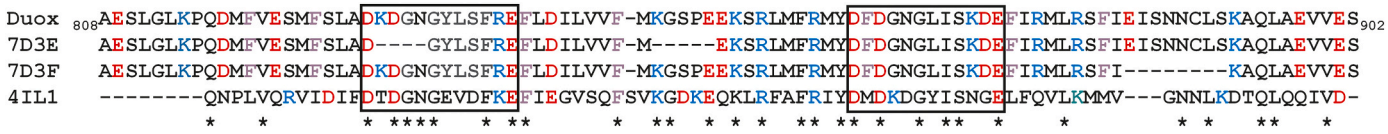

Fig. 1. The Sequence of Duox's EFD_S. The sequences labeled 7D3E and 7D3F were adapted from the structures obtained via Cryo-EM (Reference 28) for low and high concentrations of Ca^{2+}, respectively. Dashed lines represent peptide sequences that were not visible in Cryo-EM. The EF-loops are enclosed in boxes, while residues highlighted in red and blue indicate negatively and positively charged residues, respectively. The Phe residues in purple are nonpolar residues involved the interaction with DH. Additionally, the Ca^{2+} binding sequence of calcineurin (4IL1.pdb) is included for comparison because it shares structural similarities with Duox. The * symbol marks the residues conserved between Duox and calcineurin. (For interpretation of the references to colour in this figure legend, the reader is referred to the web version of this article.)

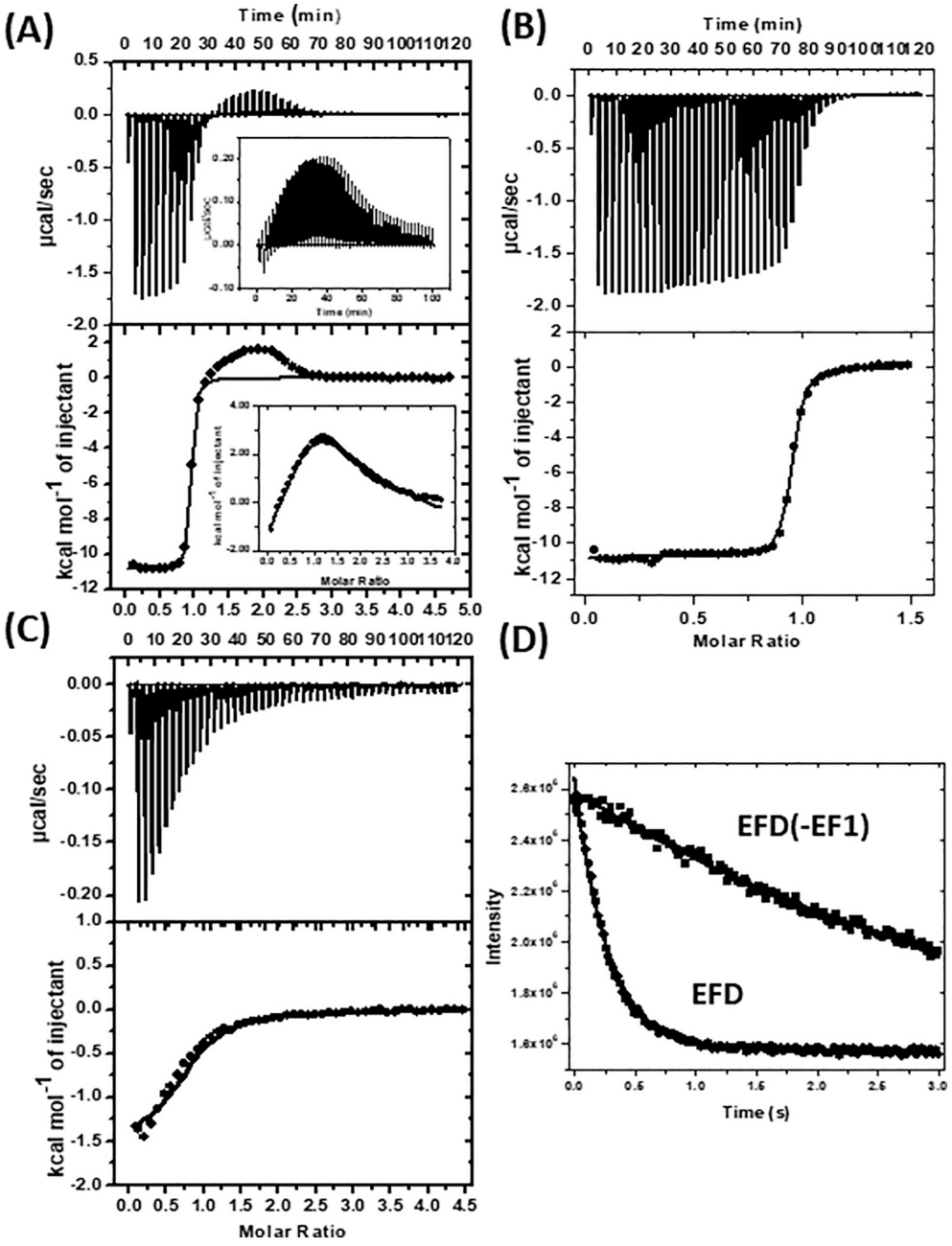

Fig. 2. Ca^{2+} Binding Thermodynamics and Kinetics. (A) A solution of Duox's EFD_S in a buffer containing 50 mM Tris, pH 7.5, was titrated with Ca^{2+} at 25 °C. The resulting binding isotherm could not be fitted with any model. Therefore, the fitting curves were performed specifically for the strong binding and weak bindings (Insert). The weak bindings were determined by intentionally saturating the high Ca^{2+} binding affinity site followed by Ca^{2+} titration. Panels (B) and (C) depict the bindings for EFD_S(-EF1) and EFD_S(-EF2), which were fitted with a "one-set-of-sites" binding model. Panel (D) shows the kinetics of Ca^{2+} dissociation by mixing Ca^{2+}-bound EFD_S or mutants with an excess of EDTA in the presence of ANS. Note the experiment for EFD_S(-EF1) was monitored for >10 s to determine the rate constant precisely. The time window was chosen for comparison. The fitting results are summarized in Table 1.

investigations should provide an answer to this outstanding question.

In cellular conditions, the concentration of Mg^{2+} is approximately 1–2 mM, which would potentially compete with Ca^{2+} if a protein contains Ca^{2+}/Mg^{2+} EF-hand(s) [11,22]. Therefore, we replaced Ca^{2+} with Mg^{2+} and performed similar solution measurement in the presence of the specific Ca^{2+}chelator, EGTA. We found that Duox's EFD_S does not bind to Mg^{2+} (data not shown).

Like other Ca^{2+}-binding proteins, the Ca^{2+} association rate constant (k_{on}) of Duox's EFD_S is extremely fast, making it impossible to be determined using our stopped-flow device. However, the slower Ca^{2+} dissociation rate constant (k_{off}) can be measured [15]. As Trp fluorescence of EFD_S was not affected by Ca^{2+} binding, we utilized ANS fluorescence to detect signal change associated with Ca^{2+} binding (refer to text below). ANS, a fluorescent probe that is commonly used to assess the hydrophobicity content of a protein, serves as an indicator for conformational change of EFD_S upon Ca^{2+} dissociation. To this purpose, ANS release from a protein must occur much faster than the conformational change. In other words, the ANS dissociation cannot be a rate determining step (RDS). The rapid ANS dissociation from the protein was supported by two control experiments (Fig. S1). A solution containing both BSA and ANS was mixed with a buffer to initiate ANS dissociation from the protein due to dilution, resulting in a drop in ANS intensity within ~40 ms in our experimental setting. Further, we monitored Ca^{2+} dissociation from Nox5's EFD [15], a similar acidic

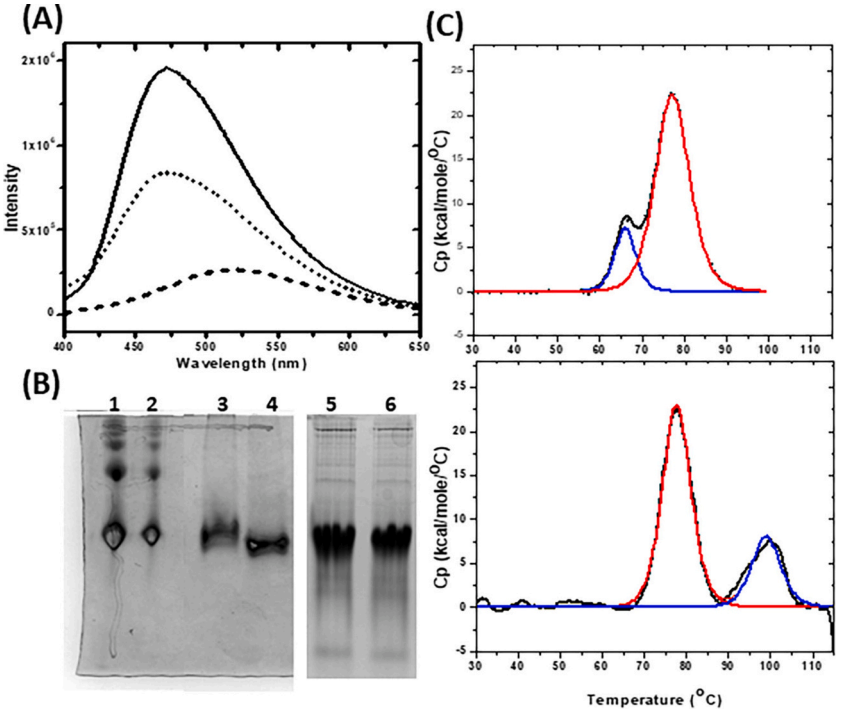

Fig. 3. Conformational Changes Assessed by ANS Fluorescence, Electrophoresis Mobility, and DSC. (A) The hydrophobicity induced by Ca^{2+} was assessed by the ANS fluorescence, which shows ANS alone (dashed line), apo EFD_S (dotted line), and Ca^{2+}-bound EFD_S (solid line). Note the significant intensity increase in the presence of EDTA was due to the ANS binding to the fused Trx protein. (B) The oligomer states and/or surface changes were determined by 12% native PAGE. Bovin serum albumin (BSA), forming monomer, dimer, trimer, and tetramer, was used a control (Lane 1 and 2). The thiol reduced EFD_S was run in the presence of Ca^{2+} (Lane 3) and EDTA (Lane 4). EFD_S(-EF1-EF2) was run under identical conditions in the presence of Ca^{2+} (Lane 5) and EDTA (Lane 6). (C) Thermograms (solid black lines) of 40 μM Duox- EFD_S in 50 mM HEPES, pH 7.5, 0.1 M NaCl in the presence of 2 mM EDTA (top panel) and 2 mM Ca^{2+} (lower panel), respectively, were fitted with non-two-state model (dotted blacked lines). The fitting of thermogram of the fused Trx protein (red line) yielded the T_m values of 77.2 and 77.7 °C and the ΔH_{unfold} values of 240 and 210 kcal/mol in the absence and presence of Ca^{2+}, respectively. The T_m values of Duox's EFD_S (blue line) were determined to be 66.9 and 99.1 °C in the absence and presence of Ca^{2+}, respectively. Note the thermogram for Ca^{2+}-bound EFD_S was not fitted well, giving less accurate T_m and enthalpy values. Aggregation producing heat (i.e., exothermic) was also observed when temperature was higher than 115 °C. (For interpretation of the references to colour in this figure legend, the reader is referred to the web version of this article.)

protein, using both Trp and ANS fluorescence, which yield compatible dissociation rate constants. Therefore, the ANS intensity change should reflect the structural change in EFD_S. When a solution of Ca^{2+}-bound EFD_S was quickly mixed with a large excess of EDTA, the ANS fluorescence was decreased exponentially, and the reaction completed in approximately 1.5 s. We fitted this decay with a single-exponential decay function, yielding a k_{off} value of 1.44 s^{-1} (Fig. 2D). The Ca^{2+} dissociation from EFD_S(-EF1) was slower, exhibiting a k_{off} value of 0.25 s^{-1}. No signal decay was detected for EFD_S(-EF2) and EFD_S(-EF1-EF2). Our data suggest that EF2 has a strong binding due to its slow Ca^{2+} dissociation.

3.3. Conformational change assessed by ANS fluorescence and electrophoretic mobility

We employed ANS molecules as a fluorescent probe to assess the protein's hydrophobicity induced by Ca^{2+} [19]. We observed Ca^{2+} binding, indicated by a notable 1.82-fold increase in ANS fluorescence at 472 nm when EFD_S was used (Fig. 3A and Table 1). EFD_S(-EF1) showed a lower intensity enhancement of approximately 1.50-fold, while EFD_S(-EF2) demonstrated a small increase in ANS intensity (Table 1). Our result indicates that the hydrophobic exposure induced by Ca^{2+} binding is greater for EF2 than for EF1.

We then investigated the Ca^{2+} bindings of EFD_S constructs by analyzing their electrophoretic mobility in a native gel. The mobility of these proteins in their native states depends on the electrostatic driving

Table 1
Ca^{2+} Binding Thermodynamics and Kinetics of EFD_S*.

Protein	ANS Enhancement	EF1			EF2			$k_{off}(s^{-1})$
		K_a (M^{-1}) (n)	ΔH_1^0 (kcal/mol)	ΔS_1^0 (cal/mol•K)	K_a (M^{-1}) (n)	ΔH_1^0 (kcal/mol)	ΔS_1^0 (cal/mol•K)	
EFD_S	1.82 ± 0.12	~ 10^5	~ 1.7		~ 10^7	~ −11		1.44 ± 0.05
EFD_S(-EF1)	1.53 ± 0.15				1.25 ± 0.16 × 10^7 (0.94 ± 0.02)	−10.83 ± 0.37	−1.15 ± 0.30	0.25 ± 0.03
EFD_S(-EF2)	1.12 ± 0.08	5.46 ± 0.59 × 10^5 (0.91 ± 0.05)	−1.22 ± 0.01	22.1 ± 0.1				n.d**
EFD_S(-EF1-EF2)	1.00 ± 0.02	n.d.	n.d.	n.d.	n.d.	n.d.	n.d.	n.d.

* The data are represented as an average plus standard deviation from at least three different measurements. The entropy change was calculated using the following equation: $\Delta G^o = -RT \ln(K_a) = \Delta H^o - T\Delta S^o$ at 25 °C.

** n.d. not detected.

force induced by the applied electric field and hydrodynamic retardation of proteins migrating within the native gel. Consequently, this mobility is influenced by a protein's surface charge, size, and shape. Mobility measurements have been utilized to study the Ca^{2+}-dependent conformational changes in various Ca^{2+}-sensor protein [23]. Trx-fused EFD_S is an acidic protein with a theoretic pI value of 4.67 because it contains a high number of negatively charged residues in Trx and EFD_S. Therefore, it migrates in an electric field under neutral buffer conditions. Despite being much smaller than BSA monomer (66 kDa), the Trx fused EFD_S (25 kDa) migrated at a comparable speed. The Ca^{2+}-bound EFD_S (Fig. 3B) and its single-substitution mutants (data not shown) migrated slower than their corresponding apo-EFD_S constructs. The slow migration suggests that the Ca^{2+} bound EFD_S either adapts a flexible structure without significant change of its surface charges or forms a structure where its negatively charged residues are buried. To differentiate between these two cases, we performed thermal unfolding studies in the absence and presence of Ca^{2+}, and our differential scanning calorimetry (DSC) data for the His-patch Trx fused EFD_S revealed two distinct peaks (Fig. 3C). The melting temperatures (T_ms) of Trx (~77 °C) closely aligned with the previously reported value (78.1 °C) determined using fluorescence [24]. A significant increase in stability was observed in the Ca^{2+}-bound EFD_S, as evidenced by an increase in T_m from 66.9 to 99.1 °C and an increase in the enthalpy of denaturation (ΔH_{unfold}) from 48 to 68 kcal/mol. Hence, the primary factor influencing the electrophoretic mobility of EFDs by Ca^{2+} is the reduction in surface negative charges. With a rigid, stable structure, as evidenced in DSC experiments, and no change in surface charges, faster migration would be anticipated. We could not determine the thermostability of all mutants, as they were precipitated during the measurements.

3.4. Size exclusion chromatography to evaluate the oligomeric state

Giving that majority of EF-hand proteins typically contain two pairs of EF-hands, a protein with only one pair of EF-hands has the potential to form a dimer, thus resulting in a total of four EF-hands, as seen in calbindin D_{9K} [25]. Therefore, we employed size exclusion chromatograph (SEC) to assess the oligomeric states of Duox's EFD_S. Three samples with the known molecular weights and oligomeric states were used as references, including BSA, cyan fluorescent protein fused N-terminal half domain of CaM (cfp-NCaM), and histidine-tagged CaM. BSA trimer, dimer, and monomer were eluted at 5.90, 6.70, and 7.64 min, respectively, while cfp-NCaM and CaM were eluted at 9.70 and 11.67 min, respectively (Fig. 4A). The reduced Trx-fused EFD_S (25 kDa) was eluted at 8.34 min, between the eluted times for BSA monomer (66 kDa) and cfp-NCaM (37 kDa), indicating that EFD_S formed a dimer in the absence of Ca^{2+} (Fig. 4B). To verify the dimerization, partially denatured EFD_S was injected to the HPLC-SEC under identical conditions. Two overlapping peaks at 9.31 and 10.95 min were observed, with the latter mainly attributed to the EFD_S monomer. Note that a single monomer species cannot be obtained, possibly because a fraction of the dissociated monomer quickly re-associated back to the dimer during chromatography (no denaturant in the HPLC buffer). We did not include a higher urea concentration for denaturation as it would compromise our HPLC system. Interestingly, a similar observation was found when the reduced EFD_S was incubated with 1–2 mM Ca^{2+}, wherein a broad peak at 9.5 min was observed, indicating a significant monomer formation. The much late elution in SEC is not attributed to the rigid structure typically formed by Ca^{2+}-bound Ca^{2+}-binding proteins (CaBPs). For example, apo and Ca^{2+}-bound cfp-NCaM were eluted 9.68 and 9.95 min, respectively (Fig. S2) while apo and Ca^{2+}-bound CaM were eluted at 11.66 and 11.97 min, respectively [20]. In both cases, there was a small change in elution time and no significant peak broadening in the presence of Ca^{2+}. We also ruled out the possibility that dimer formation was through an inter-disulfide crosslink between two EFDs molecules, based on our sample preparation described in Experimental section. Furthermore, given that bacterial Trx was reported as a monomer [26,27] and observed as such in our control experiment, we concluded that this dimerization did not involve the Trx protein. When EFD was replaced with AEDANS Cys-labeled EFD_S, the absorption and fluorescence from elute fractions were monitored, and the results were consistent with those obtained using the reduced EFD_S. Upon Ca^{2+} binding, EFD_S(-EF1) primarily exists as a monomer with an elution time of 11.16 min. On the other hand, Ca^{2+}-bound EFD_S(-EF2) exists as a major dimer form. As expected, the double Ca^{2+}-binding knockout mutant, EFD_S(-EF1-EF2), forms a dimer in the absence and presence of Ca^{2+} (data not shown). Based on our SEC result, we concluded that the elution times for the EFD_S dimer and monomer are approximately 8.34 and 11.16 min, respectively.

3.5. Dynamic light scattering (DLS)

The dimer formation observed in SEC study contradicts the finding of the electrophoretic mobility, where only a "presumably" monomer was observed. However, it is important to note that both studies were conducted under non-equilibrium systems. The oligomeric states may depend on the study systems. For example, the applied electric field in electrophoresis may disrupt dimeric interface, resulting in monomers. Therefore, we employed dynamic light scattering (DLS) to study this in an equilibrium state. We attempted to assess their oligomeric states based on the determined hydrodynamic radius (R_h) in the presence of EDTA and Ca^{2+}. Fig. 5A shows the autocorrelation function for apo-EFD_S. The fitting revealed a dominant species with an R_h value of 3.2 nm and the percentage of polydispersity (%pd) of 18.6%. The average molecular weight (MW) was determined to be ~50 kDa, assuming the structure resembled a Raliegh sphere, which is close to the anticipated MW. The plot also indicates that a smaller species (~5%) with the R_h value of ~2 nm was formed, indicating EFD_S was in equilibrium between monomer and dimer. This observation is consistent with results from the SEC. For all mutants in the absence of Ca^{2+}, their DLS spectra were similar to the apo wild type. However, we did not observe a single, smaller species as anticipated for EFD_S(-EF1) monomer. Instead, the DLS result revealed a heterogeneous mixture, with higher contents of monomer (~30%). The DLS spectrum of Ca^{2+}-bound EFD_S(-EF2) resembled that of the wild type.

3.6. Modeling

During our characterization, the structures of Duox become available through Cryo-EM studies [28,29]. Human form of Duox's EFD adopts different conformations at low and high concentrations of Ca^{2+} [28], despite the absence of Ca^{2+} density and missing peptide sequences in either the apo or holo form (Fig. 1). Nevertheless, we performed homology modeling, aiming to rationalize the results of our solution characterization. The modeling utilized the structures obtained from Cryo-EM as templates and constructed models as described previously [19]. The missing Ca^{2+} ions were added to the modeled holo form by structural alignment with Ca^{2+}-bound calcineurin (4IL1.pdb), which shares a similar structure to EFD_S. Fig. 6 displays the models for the apo and Ca^{2+}-bound EFD_S. EFD_S appears to have a unique structural arrangement for its two EFs. Typically, an EF-hand pair undergoes close-to-open configuration upon Ca^{2+} binding, as seen in the half domains of CaM. In the apo form, two helices in each EF are oriented antiparallel with interhelical angles ranging from 130° to 140°, which then become perpendicular upon Ca^{2+} binding, extending the structure and exposing hydrophobic residues. In the apo EFD_S, Helix A and B in the EF1 are oriented perpendicular to each other, while the orientation of Helix C and D in the EF2 remains similar for a typical apo EF-hand. An additional helix, Helix E, is located near the C-terminal end (Fig. 6A Upper Panel). The electrostatic potential calculation indicated significant negatively charged surfaces located near Helix A, EF2-loop, and C-terminal end (Fig. 6A Lower Panel). The accessible surface areas (ASAs) for polar and nonpolar were calculated to be 2636 and 4767 $Å^2$,

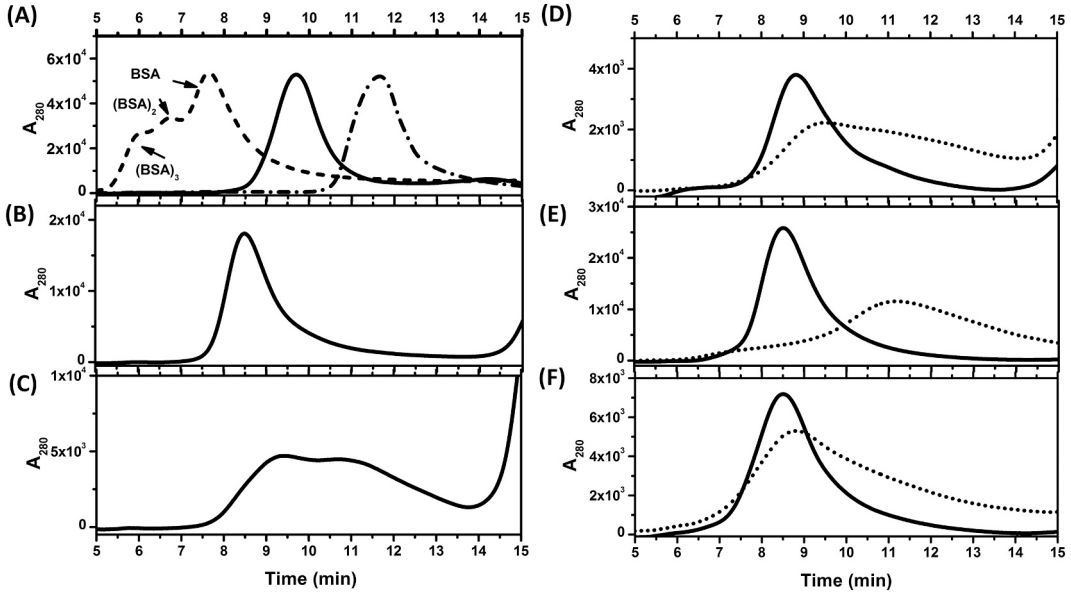

Fig. 4. Size Exclusion Chromatography of Duox's EFD_S Constructs. The SEC was conducted using an HPLC system with the running buffer (50 mM Tris, pH 7.5, 0.25 M NaCl with 2 mM Ca^{2+} or 2 mM EDTA). (A) Proteins with known molecular weights were run under identical conditions, including BSA monomer (66.5 kDa), dimer (133.0 kDa) and trimer (199.5 kDa), presented as a dashed line, cfp-NCaM (37 kDa; solid line), and CaM (20 kDa; dash-dotted line). (B) Trx-fused EFD_S (25 kDa) was run under identical conditions in the absence of Ca^{2+}. (C) The identical EFD_S denatured in 4 M urea showed two distinct peaks corresponding to the dimer and monomer. EFD_S, EFD_S(-EF1), EFD_S(-2EF) were run under identical conditions (Panels D, E, and F) in the absence of Ca^{2+} (solid lines) and presence of 2 mM Ca^{2+} (dotted lines).

respectively. Ca^{2+} binding induces the interhelical angle of Helix C and D to roughly 90° while no significant change in the angle for Helix A and B. The Ca^{2+} binding also causes the connecting loop between the two EFs to extend out, resulting in EF1 shifting approximately 60° from EF2, rendering a relative more extended structure (Fig. 6C). In such an arrangement, the distance between two Ca^{2+} ions is longer (~22 Å) than the typical EF pair (~11 Å). The ASAs for polar and nonpolar in Ca^{2+}-bound are 2314 and 4858 $Å^2$, respectively. The negatively charged surface in EF2-loop becomes significantly reduced, resulting in an overall extended structure with a predominantly negatively charged surface on one side and positively charged surface on the other side. Nevertheless, the non-polar residues are dominated in both forms. The ASA changes (ΔASAs) for polar and non-polar exposures upon Ca^{2+} change were calculated to be −325 and 91 $Å^2$, respectively.

4. Conclusion and discusion

In this study, we investigated the Ca^{2+} binding and associated conformational changes of a truncated Duox's EFD. The Ca^{2+} binding to EFD_S appears to occur sequentially, with a strong exothermic binding ($K_a = \sim 10^7\ M^{-1}$) followed by a weaker binding ($K_a = \sim 10^5\ M^{-1}$). Efforts to model the binding were not successful, possibly due to non-specific binding and/or the presence of impurities. Through mutagenesis, we showed that EF2 exhibits a high affinity for Ca^{2+}, with a molar binding enthalpy of −10.83 kcal/mol, close aligning with the values estimated from the wild type (~ −11 kcal/mol). This strong Ca^{2+} binding is attributed to the slower Ca^{2+} dissociation rate. On the other hand, EF1 has a weaker binding with a fast Ca^{2+} dissociation rate. It should be noted that the substitution of E to Q substitution in the 12th residues of each EF did affect the other EF's Ca^{2+} binding, indicating cooperativity in Ca^{2+} binding between two EFs. For example, a slower Ca^{2+} dissociation rate is observed in EFDs(-EF1) compared to the wild type. Future work will need to determine the extent of cooperativity. Furthermore, we cannot rule out the possible effect of the fused Trx protein on the Ca^{2+} binding ability of EFD_S.

Binding of a divalent ion to a protein initially involves desolvating the ion, driven by entropy gain, resulting in a positive ΔH [30]. However, the favorable process related to the Ca^{2+}-ligand interaction may lead to an overall exothermic reaction (ΔH < 0). In Ca^{2+}-EDTA titration in Tris, pH 7.5, the enthalpy change is mainly attributed to the heat release from a proton dissociated from EDTA to the buffer [31]. However, given the number of proton releases from Ca^{2+} binding to Duox's EFD is 0.12 (unpublished data), which is similar to Nox5's EFD [11]. We infer that the binding of Ca^{2+} to EF2 induces a conformation change resulting in the net formation of electrostatic interactions. On the other hand, the subsequent Ca^{2+} binding to EF1 appears to be entropy-driven due to the hydrophobic effect. Our results also indicate that Ca^{2+} binding to EFD_S leads to a reduction of surface negatively charged residues and an increase in hydrophobic exposure, consistent with the result form modeling. Such conformational change renders a stable structure with a higher melting temperature than the apo form.

An intriguing finding is that Duox's apo-EFD_S is present in a dimeric form. Upon Ca^{2+} binding, it slightly induces a shift in the oligomeric states towards the monomeric form, as observed in a non-equilibrium gel filtration process. Mutagenesis studies further suggest that the Ca^{2+}-induced conformational change of EF2 plays a pivotal role in dimer dissociation. This is supported by observations: EFD_S(-EF1) containing Ca^{2+}-bound EF2 leads to monomer formation, while EFD_S(-EF2) with Ca^{2+}-bound EF1 mostly remains in dimer formation. The possibly of a dimer-monomer equilibrium, arising from the changes of the dimer interface by divalent ions, such as Ca^{2+} and Mg^{2+}, is ruled out, as it requires an ion concentration higher than 1 M [32]. Additionally, it is important to highlight that our electrophoretic mobility measurements did not reveal any oligomeric information. However, it is possible to assign those species as monomers, as seen in CaM [23]. The absence of dimer formation might be attributed to the electric field applied during electrophoresis, which potentially causes dimer dissociation within native gels. The observation is consistent with the study using DLS, an equilibrium system, revealed that majority of EFD_S exists as a dimeric form, and Ca^{2+} binding shifts the equilibrium towards monomers. Interestingly, a predominated monomeric form of Ca^{2+}-bound EFDs (-EF1), as seen in SEC, was not observed in DLS. Instead, the content of monomer and the degree of polydispersity are higher than those of the wild type and other mutants, suggesting that the interaction between

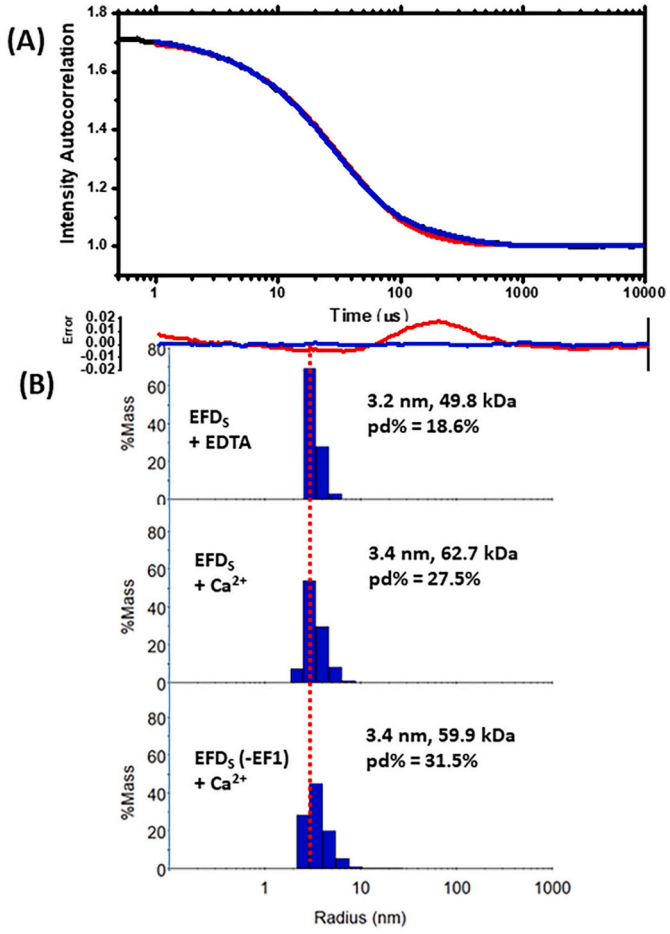

Fig. 5. Dynamic Light Scattering of Apo and Ca^{2+}-Bound Forms of EFD_S. (A) The intensity autocorrelation versus decay time (black) was obtained for 1 mg/mL EFD_S or mutants in a buffer containing 1 mM EDTA (or 2 mM Ca^{2+}) and 1–2 mM DTT. The regularization analysis (blue) yielded mean R_h and %pd. values, while Cumulants fit (red) did not fit autocorrelation well. The errors for corresponding residues are showed in the lower panel. (B) Regularization graphs were generated for EFD_S in the absence and presence of Ca^{2+}, as well as EFD_S(-EF1) in the presence of Ca^{2+} under identical conditions. The purified samples appear to contain trace amounts of impure molecule(s), as indicated in Cumulants fit. Otherwise, the samples were monomodal and polydisperse. The vertical red dashed line across the regularization graphs indicates the transition towards smaller particles. Since we do not know the shape of the Trx fused proteins, molecular wights derived from hydrodynamic radii are semi-quantitative. (For interpretation of the references to colour in this figure legend, the reader is referred to the web version of this article.)

two EFD_S(-EF1) molecules is weak. This results in a predominated monomer species in a non-equilibrium system while maintaining monomer/dimer equilibrium in an equilibrium system. Note a higher degree of disperse is commonly found in Ca^{2+}-binding proteins in DLS, such as CaM [20,33], indicating their dynamic properties.

Our solution characterization suggests that the apo EFD_S forms a dimer through hydrophobic effect, likely involving EF2. Ca^{2+} initially binds to EF2 of the dimeric EFD_S, forming a stable structure with significantly exposed hydrophobic patches and the burial of negatively charged surface areas. This disrupts the dimer interface, favoring monomer formation, resulting in a conformation resembling Ca^{2+}-EFD_S(-EF1), as depicted in Fig. 6D. The second Ca^{2+} binding event occurs at the lower Ca^{2+} binding affinity site, EF1, resulting in an extended structure. This, in turn, favors dimer formation again through hydrophobic effect, as seen in EFD_S(-EF2). This observation is consistent with a reduced hydrophobic exposure for ANS binding and a small enthalpy change (or high entropy gain). Our solution characterization, combining with modeling, reveals an interesting aspect about the region near Ca^{2+} binding sites of Duox. This region does not exhibit the typical structure of an EF-hand pair, forming dimer in apo form and undergoing an equilibrium between dimer and monomer in the presence of Ca^{2+}. A known example of such dimer formation occurs in EF-containing protein D_{9K}, a Ca^{2+} buffer protein having one EF pair that does not undergo significant conformational changes upon Ca^{2+} binding. Its structure resembles that of the apo-form of a typical EF pair. Duox's EFD appears to be an atypical EF-hand containing protein, exhibiting unique conformational and oligomeric state changes that require further investigation. In fact, EFD_S is rich in Phe residues in EF1. Therefore, we hypothesized that these Phe residues are responsible for reforming dimer in its holo state. Our recent preliminary data from the full-length EFD, showing a similar Ca^{2+}-induced oligomeric state change, support such a hypothesis.

Ca^{2+}-dependent Nox5 and Duox appear to use different activation mechanisms. Nox5's EFD consists of 4 EFs, structurally similar to CaM in terms of Ca^{2+} binding affinity and the induced conformational changes [11]. The linker sequence connecting its two half-domains is less flexible, making the whole molecule less plastic than CaM [11]. Upon Ca^{2+} binding, Nox5's EFD undergoes a conformational change to expose its hydrophobic patches, which wrap around the REFBD sequence within its DH domain, facilitating its interaction with DH and TMD domains for electron transfer among cofactors NADPH, FAD, and hemes. Since Nox5's is an oligomer, mediated by its DH domain [20,34], it is unclear whether the electron transfer occurs within the same or different polypeptide. The structure of human Duox:DuoxA1 tetramer indicates that Duox's EFD loosely associates with its DH and TMD domains in the apo form; Ca^{2+} binding renders a strong interdomain interaction, mainly through hydrophobic interactions with DH, thus facilitating electron transfer for ROS production (Fig. 7) [28]. Although the Cryo-EM derived data has not revealed the Ca^{2+} ions, the presence of Ca^{2+} ions are verified by the fact that the corresponding EF-hands region binds to DH similar to Ca^{2+}-bound phosphatase calcineurin with CaM [35]. Given that the Duox dimer within the Duox:DuoxA1 tetramer is formed through the PD domain, the EFD dimerization observed in our study could simply reflect the nature of this protein and is unlikely to play a role in Duox activation. Nevertheless, this study supports the hypothesized mechanism by providing Ca^{2+} binding affinity for each EF-hand and the associated Ca^{2+}-induced structural changes. Additionally, we identified the exposed non-polar residues near EF1 in its Ca^{2+}-bound state, which are responsible for dimer formation in our study, but they facilitate tighter binding between EFD and DH in the Duox structure. Interestingly, the study of mouse Duox revealed a contradictory activation mechanism. A tetramer formed by two Duox1:DuoxA1 complexes was also observed, except that its EFD was completely not resolved in Cryo-EM [29]. Since this tetramer is inactive, the author suggests an oligomer-mediated activation mechanism. Future investigations into the relationship between oligomers and ROS activity should provide a detailed activation mechanism. Therefore, we believe that the role of Duox's EFD in the activation mechanism remains inconclusive and requires further investigation.

Supplementary data to this article can be found online at https://doi.org/10.1016/j.bpc.2024.107271.

Declaration of generative AI in scientific writing

During the preparation of this work, the authors utilized ChatGPT (OpenAI) to aid in proofreading for readability purposes, without creating any content. All contents in this manuscript were written and thoroughly reviewed by the authors. The authors take full responsibility for the content of this publication.

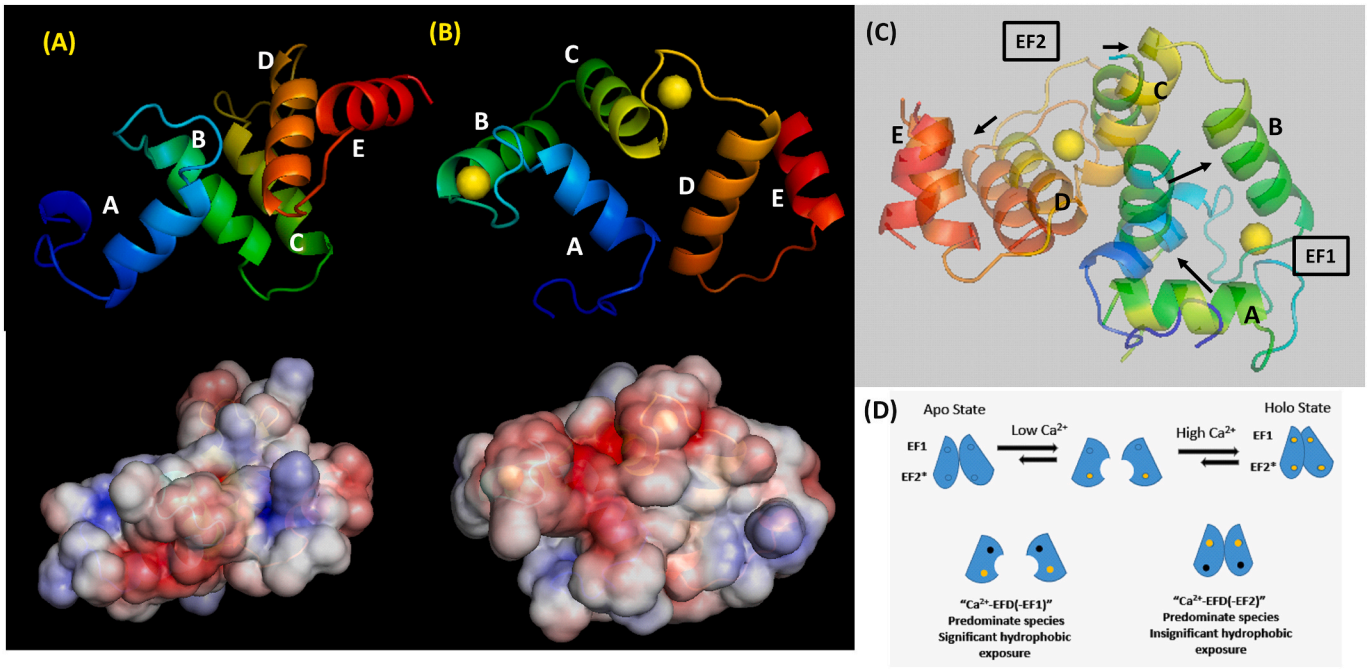

Fig. 6. Modeled Structures of Duox's EFD_S. The EFDs models were constructed via homology modeling to incorporate missing sequences in both the apo (A) and Ca^{2+}-bound (B) forms. Electrostatic potentials were computed using PyMol with the Adaptive Poisson-Boltzmann Solver (APBS) plugin. In the visual representation, red and blue surfaces present negatively and positively charged residues, respectively, while gray indicates non-polar residues. Both structures were aligned (C), with arrows highlighting the helical changes upon Ca^{2+} binding. The sequential Ca^{2+} binding to EFD_S and the consequential dimer-monomer transition are illustrated in (D). Note that the dimer structure is for presentation purposes only, as we have no information about whether the formation is in head-to-head or head-to-tail orientation. (For interpretation of the references to colour in this figure legend, the reader is referred to the web version of this article.)

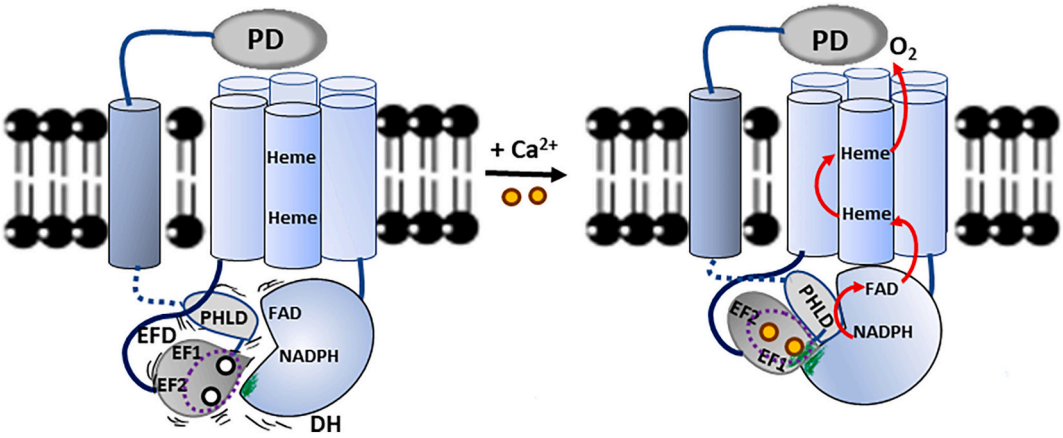

Fig. 7. The Hypothesized Activation Mechanism for Duox. Duox containing PD, TMD, EFD, and DH domains is presented as monomer here. The full-length EFD domain defined between transmembrane M0 and M1 is further divided into a Pleckstrin homology-like domain (PHLD) and EF-containing subdomains. In the Ca^{2+}-free state, these two subdomains and DH pack loosely, which does not fully engage electron transfer from NADPH to FAD to heme, resulting in little basal ROS activity. Upon binding with two Ca^{2+} ions (orange circles) to the EF-containing subdomain, the resulting conformational change decreases its negatively charged surface and exposes hydrophobic patches, which stabilize the interaction with DH primarily via the hydrophobic effect, rendering tight binding for all domains and facilitating electron transfer for ROS production. The EFD_S construct used in this study is part of EF-containing subdomain and is highlighted by dashed purple circles. The Ca^{2+} induced hydrophobic exposures of the Phe-rich region in EF1 lead to non-polar interaction with several non-polar residues of the DH domain (green shades). Ca^{2+} binding also induces hydrophobic exposure in EF2, which may further stabilize the entire EFD domain. Note that approximately 80 residues after EF2 were not resolved in Cryo-EM. The hypothesized mechanism is adapted from Ref. 28.

CRediT authorship contribution statement

Chin-Chuan Wei: Writing – review & editing, Writing – original draft, Supervision, Software, Methodology, Funding acquisition, Conceptualization. **Amena Abdul Razzak:** Writing – review & editing, Methodology, Data curation. **Hadis Ghasemi:** Writing – review & editing, Validation, Methodology, Formal analysis, Data curation. **Rahil Khedri:** Software, Resources. **Alexandria Fraase:** Writing – review & editing, Software, Resources.

Declaration of competing interest

The authors declare the following financial interests/personal relationships which may be considered as potential competing interests:

Chin-Chuan Wei reports financial support was provided by National Science Foundation. If there are other authors, they declare that they

have no known competing financial interests or personal relationships that could have appeared to influence the work reported in this paper.

Acknowledgements

We thank Quincie Hayden and Nick McDonald for helping protein purification. We thank the internal financial support from Southern Illinois University Edwardsville: Undergraduate Research and Creative Activities (URCA) to AF and Research Grants for Graduate Students (RGGS) to AR and HG.

References

[1] J.D. Lambeth, Nox/Duox family of nicotinamide adenine dinucleotide (phosphate) oxidases, Curr. Opin. Hematol. 9 (1) (2002) 11–17.
[2] S. Sorce, K.H. Krause, NOX enzymes in the central nervous system: from signaling to disease, Antioxid. Redox Signal. 11 (10) (2009) 2481–2504.
[3] C. Jha Jay, M.D. Watson Anna, G. Mathew, Lisanne C. de Vos, K. Jandeleit-Dahm, The emerging role of NADPH oxidase NOX5 in vascular disease, Clin. Sci. 131 (10) (2017) 981–990.
[4] C.E. Holterman, N.C. Read, C.R. Kennedy, Nox and renal disease, Clin. Sci. (Lond.) 128 (8) (2015) 465–481.
[5] D. Sarr, A.D. Gingerich, N.M. Asthiwi, F. Almutairi, G.A. Sautto, J. Ecker, T. Nagy, M.B. Kilgore, J.D. Chandler, T.M. Ross, et al., Dual oxidase 1 promotes antiviral innate immunity, Proc. Natl. Acad. Sci. USA 118 (26) (2021).
[6] R. Ameziane-El-Hassani, S. Morand, J.L. Boucher, Y.M. Frapart, D. Apostolou, D. Agnandji, S. Gnidehou, R. Ohayon, M.S. Noel-Hudson, J. Francon, et al., Dual oxidase-2 has an intrinsic Ca2+−dependent H2O2-generating activity, J. Biol. Chem. 280 (34) (2005) 30046–30054.
[7] H. Ohye, M. Sugawara, Dual oxidase, hydrogen peroxide and thyroid diseases, Exp. Biol. Med. (Maywood) 235 (4) (2010) 424–433.
[8] X. De Deken, B. Corvilain, J.E. Dumont, F. Miot, Roles of DUOX-mediated hydrogen peroxide in metabolism, host defense, and signaling, Antioxid. Redox Signal. 20 (17) (2014) 2776–2793.
[9] A. van der Vliet, K. Danyal, D.E. Heppner, Dual oxidase: a novel therapeutic target in allergic disease, Br. J. Pharmacol. 175 (9) (2018) 1401–1418.
[10] S. Pacquelet, M. Lehmann, S. Luxen, K. Regazzoni, M. Frausto, D. Noack, U. G. Knaus, Inhibitory action of NoxA1 on dual oxidase activity in airway cells, J. Biol. Chem. 283 (36) (2008) 24649–24658.
[11] C.C. Wei, E. Fabry, E. Hay, L. Lloyd, N. Kaufman, Y.P. Yang, D.J. Stuehr, Metal binding and conformational studies of the calcium binding domain of NADPH oxidase 5 reveal its similarity and difference to calmodulin, J. Biomol. Struct. Dyn. (2019) 1–17.
[12] F. Tirone, L. Radu, C.T. Craescu, J.A. Cox, Identification of the binding site for the regulatory calcium-binding domain in the catalytic domain of NOX5, Biochemistry 49 (4) (2010) 761–771.
[13] C.C. Wei, E. Hay, D. Smith, L. Lloyd, G. Acharya, R. Ngo, Binding of Nox5's EF-Hand domain to the peptides corresponding to the phosphorylatable region and regulatory inhibitory loop in its dehydrogenase domain, Biophys. Chem. 262 (2020) 106379.
[14] H. Grasberger, S. Refetoff, Identification of the maturation factor for dual oxidase. Evolution of an eukaryotic operon equivalent, J. Biol. Chem. 281 (27) (2006) 18269–18272.
[15] C.C. Wei, N. Motl, K. Levek, L.Q. Chen, Y.P. Yang, T. Johnson, L. Hamilton, D. J. Stuehr, Conformational states and kinetics of the calcium binding domain of NADPH oxidase 5, Open Biochem. J. 4 (2010) 59–67.
[16] C.C. Wei, N. Reynolds, C. Palka, K. Wetherell, T. Boyle, Y.P. Yang, Z.Q. Wang, D. J. Stuehr, Characterization of the 1st and 2nd EF-hands of NADPH oxidase 5 by fluorescence, isothermal titration calorimetry, and circular dichroism, Chem. Cent. J. 6 (1) (2012) 29.
[17] C.N. Pace, F. Vajdos, L. Fee, G. Grimsley, T. Gray, How to measure and predict the molar absorption coefficient of a protein, Protein Sci. 4 (11) (1995) 2411–2423.
[18] V. Mittard, N. Morelle, B. Brutscher, J.P. Simorre, D. Marion, M. Stein, J. P. Jacquot, P.N. Lirsac, J.M. Lancelin, 1H, 13C, 15N-NMR resonance assignments of oxidized thioredoxin h from the eukaryotic green alga Chlamydomonas reinhardtii using new methods based on two-dimensional triple-resonance NMR spectroscopy and computer-assisted backbone assignment, Eur. J. Biochem. 229 (2) (1995) 473–485.
[19] D. Jensen, N. Reynolds, Y.P. Yang, S. Shakya, Z.Q. Wang, D.J. Stuehr, C.C. Wei, The exchanged EF-hands in calmodulin and troponin C chimeras impair the Ca(2)(+)-induced hydrophobicity and alter the interaction with Orai1: a spectroscopic, thermodynamic and kinetic study, BMC Biochem. 16 (2015) 6.
[20] D. Smith, L. Lloyd, E. Wei, P. Radmanesh, C.C. Wei, Calmodulin binding to the dehydrogenase domain of NADPH oxidase 5 alters its oligomeric state, Biochem. Biophys. Rep. 29 (2022) 101198.
[21] S. Rigutto, C. Hoste, H. Grasberger, M. Milenkovic, D. Communi, J.E. Dumont, B. Corvilain, F. Miot, X. De Deken, Activation of dual oxidases Duox1 and Duox2: differential regulation mediated by camp-dependent protein kinase and protein kinase C-dependent phosphorylation, J. Biol. Chem. 284 (11) (2009) 6725–6734.
[22] J.L. Gifford, M.P. Walsh, H.J. Vogel, Structures and metal-ion-binding properties of the Ca2+−binding helix-loop-helix EF-hand motifs, Biochem. J. 405 (2) (2007) 199–221.
[23] J. Viviano, A. Krishnan, H. Wu, V. Venkataraman, Electrophoretic mobility shift in native gels indicates calcium-dependent structural changes of neuronal calcium sensor proteins, Anal. Biochem. 494 (2016) 93–100.
[24] Z. Lu, E.A. DiBlasio-Smith, K.L. Grant, N.W. Warne, E.R. LaVallie, L.A. Collins-Racie, M.T. Follettie, M.J. Williamson, J.M. McCoy, Histidine patch thioredoxins: mutant forms of thioredoxin with metal chelating affinity that provide for convenient purifications of thioredoxin fusion proteins (*), J. Biol. Chem. 271 (9) (1996) 5059–5065.
[25] E.L. Arévalo-Salina, J. Osuna, H. Flores, G. Saab-Rincon, Engineering a calcium-dependent conformational change in Calbindin D9k by secondary elements replacement, Arch. Biochem. Biophys. 714 (2021) 109065.
[26] J. Santos, C. Marino-Buslje, C. Kleinman, M.R. Ermacora, J.M. Delfino, Consolidation of the thioredoxin fold by peptide recognition: interaction between E. coli thioredoxin fragments 1-93 and 94-108, Biochemistry 46 (17) (2007) 5148–5159.
[27] S.K. Katti, D.M. LeMaster, H. Eklund, Crystal structure of thioredoxin from Escherichia coli at 1.68 Å resolution, J. Mol. Biol. 212 (1) (1990) 167–184.
[28] J.X. Wu, R. Liu, K. Song, L. Chen, Structures of human dual oxidase 1 complex in low-calcium and high-calcium states, Nat. Commun. 12 (1) (2021) 155.
[29] J. Sun, Structures of mouse DUOX1-DUOXA1 provide mechanistic insights into enzyme activation and regulation, Nat. Struct. Mol. Biol. 27 (11) (2020) 1086–1093.
[30] M.T. Henzl, J.D. Larson, S. Agah, Estimation of parvalbumin Ca2+− and Mg2+−binding constants by global least-squares analysis of isothermal titration calorimetry data, Anal. Biochem. 319 (2) (2003) 216–233.
[31] Y.V. Griko, Energetics of Ca(2+)-EDTA interactions: calorimetric study, Biophys. Chem. 79 (2) (1999) 117–127.
[32] M.S. Akhtar, A. Ahmad, V. Bhakuni, Divalent cation induced changes in structural properties of the dimeric enzyme glucose oxidase: dual effect of dimer stabilization and dissociation with loss of cooperative interactions in enzyme monomer, Biochemistry 41 (22) (2002) 7142–7149.
[33] A.L. Papish, L.W. Tari, H.J. Vogel, Dynamic light scattering study of calmodulin-target peptide complexes, Biophys. J. 83 (3) (2002) 1455–1464.
[34] T. Kawahara, H.M. Jackson, S.M. Smith, P.D. Simpson, J.D. Lambeth, Nox5 forms a functional oligomer mediated by self-association of its dehydrogenase domain, Biochemistry 50 (12) (2011) 2013–2025.
[35] Q. Ye, Y. Feng, Y. Yin, F. Faucher, M.A. Currie, M.N. Rahman, J. Jin, S. Li, Q. Wei, Z. Jia, Structural basis of calcineurin activation by calmodulin, Cell. Signal. 25 (12) (2013) 2661–2667.